Bilayer orthogonal ferromagnetism in CrTe2-based van der Waals system

Chiara Bigi, Cyriack Jego, Vincent Polewczyk, Alessandro de Vita, Thomas Jaouen, Hulerich Camel Tchouekem, François Bertran, Patrick Le Fèvre, Pascal Turban, Jean-Francois Jacquot, et al.

nature communications

Article

https://doi.org/10.1038/s41467-025-59266-4

Bilayer orthogonal ferromagnetism in $CrTe_2$-based van der Waals system

Received: 29 July 2024

Accepted: 11 April 2025

Published online: 14 May 2025

Check for updates

Chiara Bigi[1,17] ✉, Cyriack Jego[2,17], Vincent Polewczyk[2,3,17], Alessandro De Vita[4,5], Thomas Jaouen[6], Hulerich C. Tchouekem[6], François Bertran[1], Patrick Le Fèvre[6], Pascal Turban[6], Jean-François Jacquot[7], Jill A. Miwa[8], Oliver J. Clark[9], Anupam Jana[10], Sandeep Kumar Chaluvadi[10], Pasquale Orgiani[10], Mario Cuoco[11], Mats Leandersson[12], Thiagarajan Balasubramanian[12], Thomas Olsen[13] ✉, Younghun Hwang[14] ✉, Matthieu Jamet[2] ✉ & Federico Mazzola[15,16] ✉

Systems with pronounced spin anisotropy are pivotal in advancing magnetization switching and spin-wave generation mechanisms that are fundamental to spintronic technologies. Quasi-van der Waals ferromagnets like $Cr_{1+\delta}Te_2$ represent seminal materials in this field, renowned for their delicate balance between frustrated layered geometries and magnetism. Despite extensive investigation, the nature of their magnetic ground state and the mechanism of spin reorientation under external fields and varying temperatures remain contested. Here, we exploit complementary techniques to reveal a previously overlooked magnetic phase in $Cr_{1+\delta}Te_2$ ($\delta = 0.25 - 0.50$), which we term orthogonal-ferromagnetism. This phase consists of atomically sharp single layers of in-plane and out-of-plane maximally canted ferromagnetic blocks, which differs from the stacking of multiple heterostructural elements required for crossed magnetism. Contrary to earlier reports of gradual spin reorientation in $CrTe_2$-based systems, we present evidence for abrupt spin-flop-like transitions. This discovery further highlights $Cr_{1+\delta}Te_2$ compounds as promising candidates for spintronic and orbitronic applications, opening new pathways for device engineering.

$Cr_{1+\delta}Te_2$ transition metal dichalcogenides (TMDs) have emerged as a key platform for exploring magnetism in low-dimensions, offering several opportunities for discovering novel quantum phases[1–17]. The properties of $Cr_{1+\delta}Te_2$ are complex and can be tuned chemically via self-intercalation (see Fig. 1a). During the growth process, the Cr concentration can be controlled, with excess Cr atoms positioned within the material's van der Waals gaps. This allows precise tuning of both the magnetic and electronic properties. Among self-intercalated Cr-based materials, $Cr_{1.25}Te_2$ remains an unresolved area of study. This phase, stabilized by a 25% excess of Cr intercalated within the van der Waals gaps (Fig. 1a), exhibits magnetic behavior that has been interpreted in diverging ways in the literature. Tang et al. characterized $Cr_{1.25}Te_2$ as a ferromagnet with a pronounced out-of-plane spin polarization, suggesting well-defined magnetic order[18]. In contrast, Liu et al. identified the same material as exhibiting a mildly canted ferromagnetic structure[19].

Discrepancies also emerge when considering the dynamic behavior of magnetic moments under external magnetic fields and varying temperatures. While a continuous reordering of such moments was previously observed, a downturn in magnetization raises questions about the underlying thermodynamic processes[19]. Such conflicting behaviors suggest that $Cr_{1.25}Te_2$ exhibits a heightened sensitivity to

A full list of affiliations appears at the end of the paper. ✉e-mail: chiara.bigi@synchrotron-soleil.fr; tolsen@fysik.dtu.dk; younghh@uc.ac.kr; matthieu.jamet@cea.frt; federico.mazzola@spin.cnr.it

https://doi.org/10.1038/s41467-025-59266-4

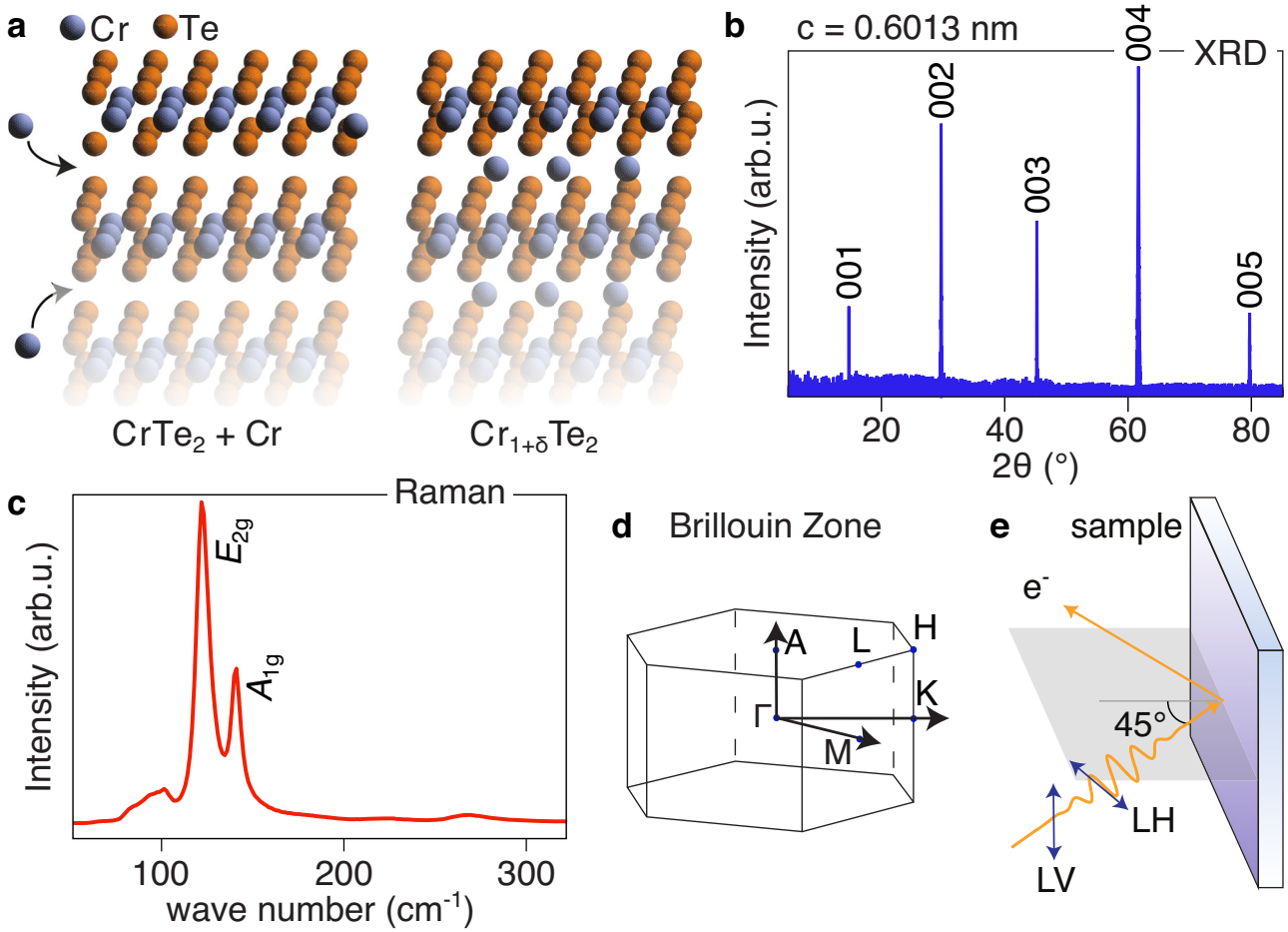

Fig. 1 | Crystalline structure of $Cr_{1+\delta}Te_2$. a Schematic of the crystal structure of $Cr_{1+\delta}Te_2$ highlighting the self-intercalation of extra Cr atoms within the van der Waals gap of the pure $CrTe_2$. **b** The *c*-axis lattice parameter obtained by x-ray diffraction (XRD) on high-quality single crystals is consistent with $\delta = 0.25$[25]. **c** Raman spectroscopy measurements reporting the E_{2g} and A_{1g} phonon manifolds with narrow lines, further corroborates the 1.25:2 stoichiometry[45]. **d** Brillouin zone **e** Cartoon of the experimental geometry and light polarization vectors used for ARPES measurements.

perturbations, such as for example, possible Cr vacancies. Further complications in defining the properties of the idealized trigonal phase arise from the several magnetic transition temperatures reported in literature. This variability suggests that the observed magnetic behavior may be modulated by subtle structural factors. As a result, pure trigonal $Cr_{1.25}Te_2$ emerges as an intriguing system—not only for its complex magnetic ordering but also for studying a nearly-ideal platform and its underlying physical mechanisms governing the thermodynamic behavior of the magnetic moments. Unraveling these complexities would mark a significant advance in understanding magnetism in TMDs, potentially uncovering new magnetic phenomena in related systems.

Herein, we synthesize high-purity single crystals of $Cr_{1.25}Te_2$ in the trigonal phase, and combine superconducting quantum interference device (SQUID) magnetometry, spin- and angle-resolved photoelectron spectroscopy (Spin-ARPES), and density functional theory (DFT) calculations, to uncover a novel magnetic ground state, with alternating maximally canted ferromagnetic orders. For simplicity, we will refer to this phase as orthogonal ferromagnetism. This emergent phase is defined by the coexistence of alternating in-plane and out-of-plane ferromagnetic moments, coupled through a significant antiferromagnetic exchange interaction, and differs in nature from crossed magnetism, exclusively achievable by stacking multiple heterostructural elements together, or grown as thin-films[20–24]. Indeed, orthogonal magnetism manifests as a single phase with alternating ferromagnetic stacking at the atomic scale, thus, interfacial problems of typical crossed magnets may be surpassed. Under an applied magnetic field, the system undergoes a pronounced, abrupt reordering, strikingly reminiscent of spin-flop transitions, marking a clear departure from what previously observed. Remarkably, this orthogonal ferromagnetic state demonstrates exceptional robustness, persisting across Cr doping levels up to at least 50%. These findings resolve discrepancies in the literature concerning the magnetic behavior of $Cr_{1+\delta}Te_2$, and place this material as a promising platform for future magnetic switching technologies.

Results

Single crystals of $Cr_{1.25}Te_2$ were synthesized via the vertical temperature gradient Bridgman method, employing ultra-high purity Cr (99.99 %) and Te (99.99999 %) as starting materials ($Cr_{1.50}Te_2$ was also grown using the same methodology; the phase and composition were checked via XRD and X-ray core level spectroscopy, respectively). Details of the growth are described in the Methods section. Structural characterization demonstrated excellent agreement with

https://doi.org/10.1038/s41467-025-59266-4

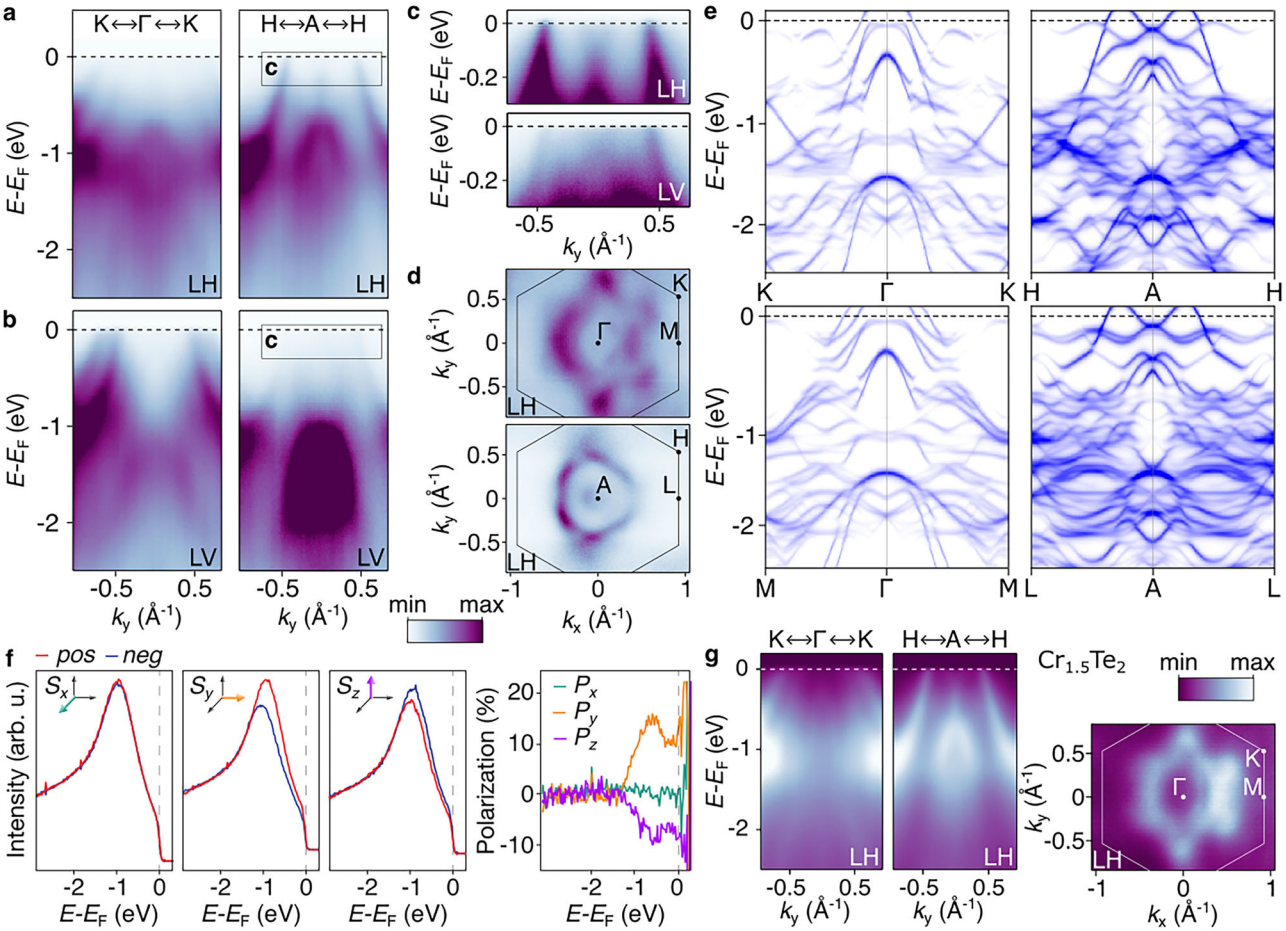

Fig. 2 | Electronic structure of $Cr_{1+\delta}Te_2$. **a** $Cr_{1.25}Te_2$ Band dispersions acquired along the $\Gamma - K$ ($h\nu = 60$ eV) and $A - H$ ($h\nu = 80$ eV) high symmetry directions with linear horizontal (LH) light polarization. **b** Same set probed with linear vertical (LV) light polarization to uncover the orbital mixing at the Fermi level. **c** The electron pocket at the Fermi level is well captured by our ab-initio calculations and allowed us to estimate an inner potential of 8 eV. **d** Fermi surface maps probed with (*top*) 60 eV and (*bottom*) 80 eV photon energies, corresponding to the bulk Brillouin zone center ($\Gamma - K - M$) and the Brillouin zone boundary ($A - H - L$), respectively. **e** Band structure calculations along $\Gamma - K$, $\Gamma - M$, $A - H$ and $A - L$ high symmetry directions. **f** Vectorial micro-spin spectroscopy performed at the Γ point ($h\nu = 100$ eV) the resulting polarization vector is consistent with the magnetic ground state of our model. **g** Electronic structure of the $Cr_{1.5}Te_2$ sister compound which displays similar magnetic behavior.

other works[25]. Notably, XRD analysis revealed a *c*-axis lattice parameter of $Cr_{1.25}Te_2$ as large as 0.6013 nm—slightly contracted relative to pure $CrTe_2$[6]—suggesting a clear structural impact from Cr intercalation and enhanced interlayer coupling (Fig. 1b). The Raman spectra on this system exhibited pronounced E_{2g} and A_{1g} phonon modes, confirming the high crystallinity and quality of the synthesized crystals (Fig. 1c).

We integrated the structural insights from XRD and Raman spectroscopy with first-principles density functional theory (DFT) calculations to survey the low-temperature magnetic ground state configurations of such systems and, as a consequence, the relevant electronic structure. The model structure is a 2×2 supercell with 2 intercalated Cr atoms arranged in a hexagonal lattice, fully consistent with the expected symmetry and geometry of the hexagonal Brillouin zone (Fig. 1d). The magnetic ground state consists of an alternating stacking of in-plane/out-of plane ferromagnetic layers at the Cr intercalated/$CrTe_2$ planes, respectively (see below and in supplementary for further details). The results reproduced the experimentally observed electronic structure at 15–20 K, as revealed by angle-resolved photoemission spectroscopy (ARPES, Fig. 2 a–e).

The ARPES and DFT calculations are compared in Fig. 2. The experimental electronic structure is marked by bands exhibiting pronounced anisotropic orbital character, with significant dispersion along k_z, indicative of moderate interlayer coupling and notable overlap of electron wavefunctions along the *c*-axis. The mixed orbital nature can be demonstrated by tuning the light polarization between linear horizontal (LH) and linear vertical (LV) (See Fig. 1e), effectively probing differently the even and odd symmetries of the orbitals during the photoemission process, from an initial to a final state[26–31]. By doing this, we observed strong changes in the spectral intensity, characterized by a major contribution from LV, which enhances primarily in-plane orbitals, for hole-like bands that disperse across the Fermi level and having their maxima above it (Fig. 2b). In contrast, LH reveals parabolic features with maxima at circa -1.2 eV below the Fermi level (Fig. 2a). According to our calculations, the states responsible for the transport properties, hence crossing the Fermi level, have an orbital contribution of roughly 50% Te *p*-states and 50% Cr states (2/3 *d*-states and 1/3 *p*-states), with similar weights across the entire Brillouin zone (see supplementary Fig. S4).

The three-dimensionality of the electronic states is evidenced by the appearance of new spectral features when changing photon energy. The latter process corresponds to effectively changing k_z and probe how the electronic structure evolves along that direction. Around the *A* point of the Brillouin zone, ARPES shows the presence of an electron-like band (Fig. 2c), also captured by the DFT calculations of the magnetic phase in Fig. 2e. Such an electron pocket crosses the

https://doi.org/10.1038/s41467-025-59266-4

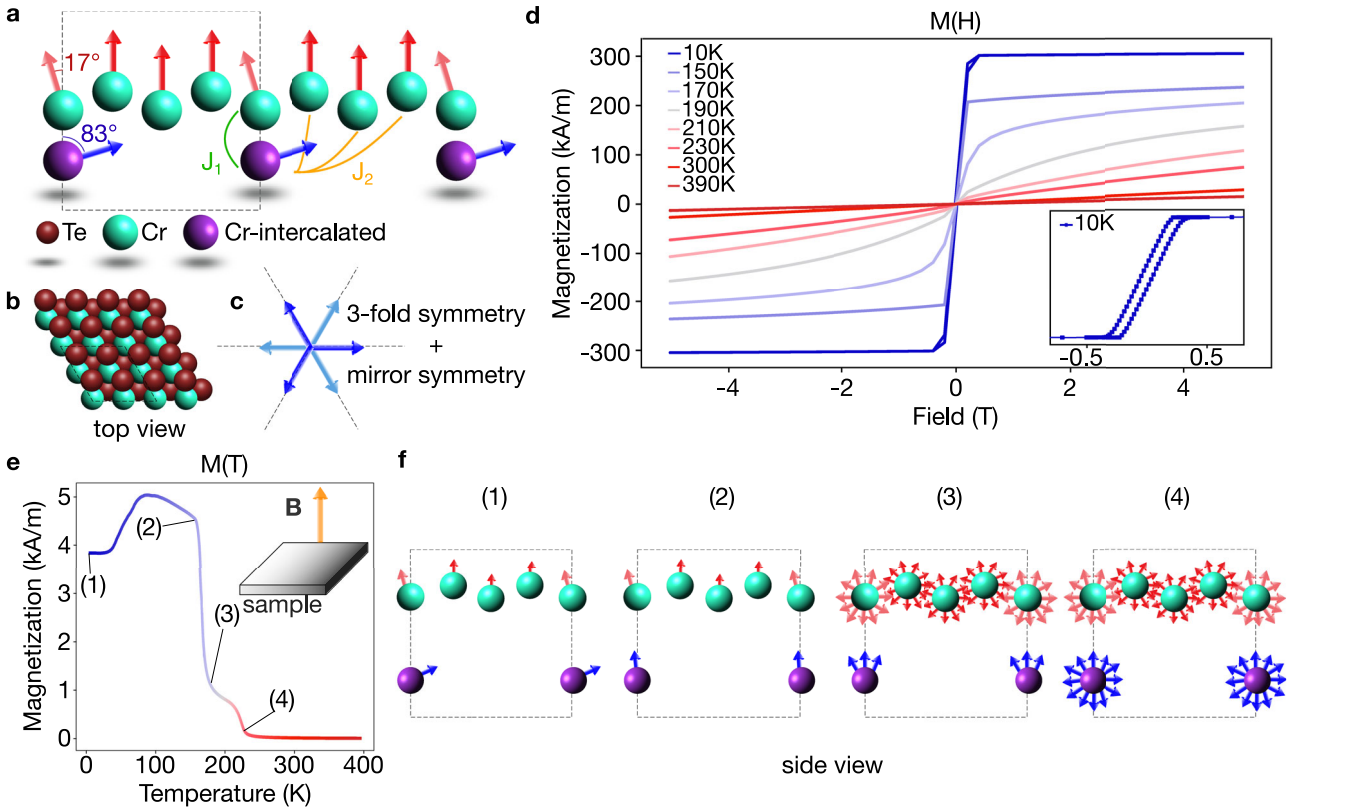

Fig. 3 | Magnetic ground state in $Cr_{1.25}Te_2$. **a** Side view of the Cr atoms arrangement in the 2 × 2 supercell (dashed lines). Light blue Cr-atoms belong to the $CrTe_2$ layers. Their magnetic moments are aligned ferromagnetically out-of-plane with a 17° canting of the Cr atoms sitting on top of the Cr intercalated within the $CrTe_2$ van der Waals gap (purple color). The magnetic moment of the intercalated atom is nearly transverse to the out-of-plane direction with a canting of 83°. The nearest-neighbors and the next-nearest-neighbors exchange interactions J_i considered in this work are also shown. **b** Top view of the crystal structure with the unit cell (dashed lines) and (**c**) in-plane spin component of the intercalated Cr resulting in three equivalent minima of the magnetic ground state. **d** Field dependent magnetization curves measured at different sample temperatures. Magnetic field was applied out of the plane of the sample. The inset shows an hysteresis acquired with smaller magnetic field steps on a different crystal piece of the same batch. We observed the same trend consistently across the various samples we probed, with only a narrow dispersion in the coercive fields (20–40 mT) and in the remanence (7–18%). **e** Magnetization as a function of temperature for an out-of-plane applied field of 3 mT and (**f**) associated sketches of the magnetization mechanism.

Fermi level and has a minimum at approximately 200 meV below it (see also Supplementary Fig. S2). Such a feature disperses with decreasing photon energy and it disappears completely at the Γ point. In contrast to the behavior of the electron pocket just described, variation in photon energy (Fig. 2c and supplementary information figures S5, S6 and S7) reveals minimal shifts in the outer hole bands which cross the Fermi level at k-points near ± 0.5 Å^{-1}, consistent with the system's intrinsic quasi-two-dimensional van der Waals nature, and underscoring the system's electronic structure, blending two-dimensional van der Waals layers with three-dimensional electronic structures.

Overall the ARPES results are consistent with the band structure obtained from our magnetic DFT calculations. Notably, non-magnetic calculations (see Supplementary Fig. S1) were inconsistent with experimental results. The presence of finite magnetic order both along the in-plane and out-of-plane directions is further strengthened by spin-ARPES data collected for three spatial components (S_x, S_y, and S_z) at the Γ point (Fig. 2f). In adherence to time-reversal symmetry, no net spin polarization should theoretically exist at this point in the absence of magnetic ordering. Nonetheless, our measurements uncover a clear violation of this symmetry, revealing both in-plane and out-of-plane spin components (Fig. 2f), in line with our theoretical predictions for the ground state. These measurements were only possible by using a micro-focused beam (lateral spot size of 10 μm) and likely magnetic domains comparable to the spot size, a hypothesis supported by previous photoemission electron microscopy (PEEM) results[7,32]. Alternatively, the measurements probed a higher proportion of domains with the same spin orientation. It is important to stress that while spin-ARPES clearly shows the breaking of time-reversal symmetry for both in-plane and out-of-plane components, these measurements are local and restricted at selected k-points, thus a one-to-one correspondence between them and the total magnetization cannot be made. Nevertheless, it corroborates the necessity of incorporating magnetic order in our model. Lastly, we extended our ARPES experiments and DFT simulations to systems with doping levels up to 50% (see Fig. 2g): as also described in the supplementary information (figure S10 and figure S11–S14), similar conclusions can be drawn up to this level of intercalated atoms, showing that orthogonal ferromagnetism is a robust and pervasive feature across a wide doping range.

The precise magnetic ground state configuration was pinpointed by testing different initial non-collinear configurations in a 2 × 2 supercell featuring a hexagonal lattice of two intercalated Cr atoms. The DFT calculations (including spin-orbit coupling) were initialized with out-of-plane ferromagnetic order for the Cr in the $CrTe_2$ layers, while the magnetic moment of the intercalated Cr atoms was tilted by a starting angle φ_i and then let evolve up to the minimization of the total energy. With this approach, we were able to identify the arrangement shown in Fig. 3a as the most favorable one (see supplementary Fig. S3 for further details). This magnetic order features alternating ferromagnetic layers on the atomic scale, with the magnetic moments oriented orthogonally between adjacent planes—a

structure which clearly differs from full ferromagnetism and that could be regarded as a maximal canted ferromagnetism (90° canting angle). According to the calculations, the intercalated Cr atoms exhibit 17° tilt from their planar configuration. This deviation is mirrored in the magnetic moments of adjacent Cr atoms, situated directly above and below the intercalated atoms in neighboring layers (one atom every four), which tilt relative to their vertical orientation by the same degree. This tilting disrupts local symmetry, introducing magnetic frustration within the $CrTe_2$ layers. The energy difference between the out-of-plane spins in the $CrTe_2$ layers and the in-plane spins in the intercalated Cr atoms is calculated to be 8 meV per unit cell. This pronounced magnetic anisotropy is likely driven by the spin-orbit coupling of the heavy, non-magnetic Te atoms. The computed total magnetization vector is [2.8, 0.0, 11.1]μ_B/fu, with individual Cr atoms exhibiting local magnetic moments of approximately 2.8 μ_B. Utilizing the classical spin model, $E = -\frac{1}{2}\sum_{ij} J_{ij}\mathbf{u}_i \cdot \mathbf{u}_j$, where $\mathbf{u}_i$ represents the unit vector of the spin direction for Cr atom i and J_{ij} denotes the exchange interaction energy, we calculate a ferromagnetic exchange between neighboring intercalated Cr atoms, with an interaction energy of J_{int} = 4 meV. Considering six nearest-neighbor interactions, we estimate a mean-field Curie temperature of approximately 90 K for magnetic ordering among the intercalated atoms. However, a more detailed analysis is necessary to provide a rigorous quantitative assessment[33], which lies beyond the scope of this study. Furthermore, we determine that the nearest-neighbor exchange interaction between the intercalated Cr atoms and those in the $CrTe_2$ layer is $J_1 = -106$ meV, while the next-nearest interaction is $J_2 = 8$ meV. This results in an effective in-plane antiferromagnetic exchange ($J_{\mathrm{eff}} = J_1 + 6J_2 < 0$) between the intercalated atoms and the $CrTe_2$ layers. Such a situation is schematically illustrated in Fig. 3a. The observed preference for transverse magnetic alignment is attributed to long-range interactions between the intercalated atoms and the $CrTe_2$ layers, further enriching the understanding on the magnetic behavior in this system.

Orthogonal-ferromagnetic systems with antiferromagnetic exchange present natural heterostructures, exhibiting pronounced anisotropic thermodynamic behavior when comparing in-plane and out-of-plane magnetic alignments. To explore this anisotropy, we examine the temperature and magnetic-field dependencies along these orthogonal directions. For fields applied out-of-plane, SQUID magnetometry reveals that below the magnetic ordering temperature, the magnetization curves (Fig. 3d) display square hysteresis loops, characterized by a small coercive field of 13 mT and a remanence approximately 7% of the saturation magnetization. This behavior is typical of systems with an easy out-of-plane magnetic axis with weak nucleation field. The effective magnetic anisotropy field is estimated at 0.6 MJ/m^3 at 150 K and 0.4 MJ/m^3 at 170 K (see Supplementary Fig. S9), comparable to values observed in perpendicular magnetic anisotropy materials such as Fe_3GeTe_2 (0.8 MJ/m^3 [34]) and CoFeB/MgO (0.5 MJ/m^3 [35]). From the saturation magnetization, the magnetic moment per Cr atom is calculated to be 2.2 ± 0.3 μ_B, lower than the theoretical value of 2.8 μ_B. This discrepancy likely reflects a lower bound, given that full saturation may not be achieved even at 5 Tesla. Additionally, paramagnetic slopes are observed at temperatures exceeding 240 K, indicative of the transition from ferromagnetic to paramagnetic behavior.

Further insights into the out-of-plane ferromagnetic order are gained by plotting the temperature-dependent magnetization under a fixed out-of-plane magnetic field of 3 mT, capturing the system's remanent state after low-temperature saturation at 5 Tesla (Fig. 3e). As shown in Fig. 3f (1) at low temperatures (10–20 K), $Cr_{1.25}Te_2$ retains its out-of-plane magnetic configuration, consistent with the schematic in Fig. 3b. As the temperature increases, (2) the magnetization exhibits a broad peak, signaling a weakening of the magnetic order. The applied magnetic field forces the moments, including those of intercalated Cr atoms, to align with the field. We note here that this interpretation is supported quantitatively by our SQUID data. Indeed, considering the same spin moment for all the Cr atoms (2.8 μ_B as evaluated by theory and 2.2 μ_B as experimentally obtained), it is readily seen that the magnetic signal of the intercalated Cr atoms would be 1/4 of the one given by the $CrTe_2$ layers. In good agreement with this, the total magnetization found by SQUID (at spin configuration (2)) is 5 kA/m, from which the intercalated Cr contribution of 1 kA/m is extracted from the difference between the magnetic signals in the spin configuration (2) and the spin configuration (1), where the remaining 4 kA/m come from the Cr atoms in the $CrTe_2$ layers. At higher temperatures, a double-hump structure appears in the magnetization curve, reflecting the progressive loss of ferromagnetic order and the emergence of paramagnetic behavior: (3) initially, the magnetic order vanishes in $CrTe_2$ planes, leading to a sharp drop in magnetization. (4) Subsequently, the intercalated Cr moments randomize, resulting in paramagnetism above 240 K.

Along the in-plane direction, we observe a more complex and unprecedented magnetic behavior in these systems. Notably, the magnetization does not reach saturation, even at low temperatures (Fig. 4a), and the curves (spanning 10 K to 150 K) exhibit a distinct change in convexity, manifesting as a characteristic 'kink'. This feature signals a sudden spin state reorientation, where the magnetic moment reverses direction, shifting from an upward to a downward configuration. This behavior sharply contrasts with previous reports on this compound, where the spins were believed to undergo a smooth reorientation with no abrupt transitions as a function of the applied magnetic field[19]. While earlier studies struggled to explain a downturn in magnetization and deemed it inconsistent with a gradual reorientation, the abrupt changes observed in our data now reconcile this feature providing a more accurate representation of the spin dynamics at play in this system (see also additional data in Supplementary Figs. S8 and S9).

To clarify the observed spin reorientation, we refer to the schematic in Fig. 4b. For simplicity, we begin by considering the ground state configuration, labeled '4', under a positive in-plane magnetic field. A similar process occurs for a negative in-plane magnetic field, following a trajectory from '3' to '1'. In the ground state (4), the Cr magnetic moments exhibit a tilt, as previously described. The in-plane magnetic components, primarily contributed by the intercalated Cr atoms, show hexagonal symmetry due to the interplay between rotated magnetic domains and the presence of three energy minima (indicated by blue arrows in the top view). Upon applying a magnetic field (5), the in-plane magnetic moments align with the field direction, resulting in the formation of a single magnetic domain. This alignment corresponds to the first spin reorientation and is reflected in the initial slope change of the magnetization curves in Fig. 4a. As the magnetic field increases, (6) all magnetic domains fully align with the applied field, and a spin-flop-like transition occurs, producing a second slope in the magnetization versus magnetic field curves. Finally, (7) all spins rotate continuously to align with the field direction. This double spin reorientation, reminiscent of spin-flop dynamics, is also observed in $Cr_{1.50}Te_2$, extending these magnetic properties to systems with up to 50% Cr doping (Supplementary Fig. S10). Moreover, this behavior stands in contrast to earlier observations, where Cr vacancies were believed to play a critical role in shaping the magnetic response. Here, we propose that the high crystallinity and large domain sizes—further corroborated by the sharp, well-defined ARPES data—reposition this system as a promising candidate for spin-flop generation.

In summary, this study unveils a magnetic ground state in $Cr_{1+\delta}Te_2$ (with δ = 0.25 – 0.50) that we term orthogonal ferromagnetism, characterized by alternating in-plane and out-of-plane ferromagnetic atomic layers coupled via antiferromagnetic exchange coupling. Our comprehensive approach, integrating SQUID magnetometry, spin-ARPES, and DFT calculations, provides definitive evidence for a previously overlooked magnetic ordering and resolves ambiguities

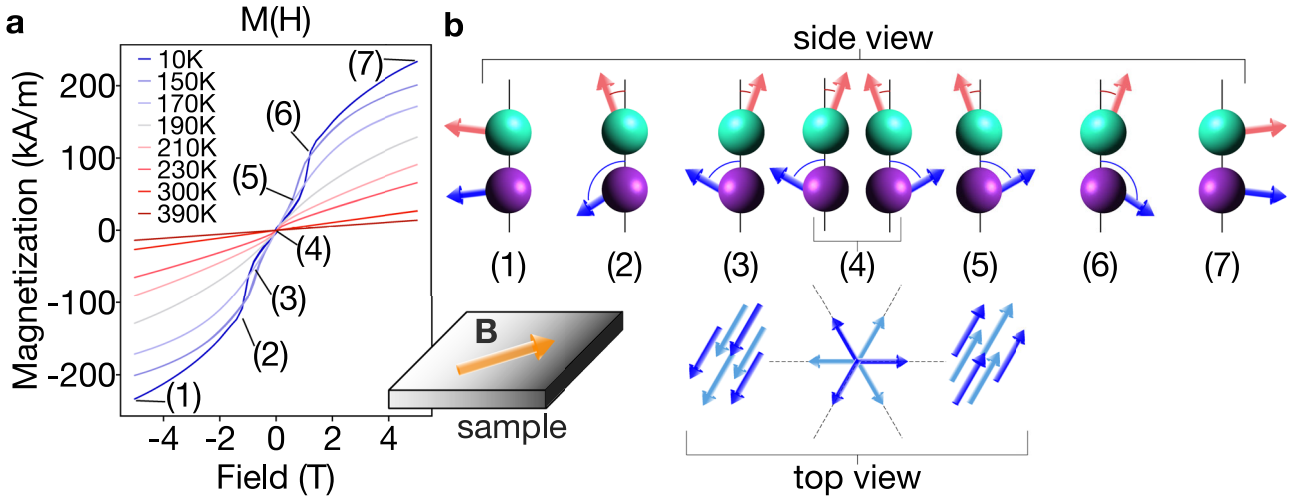

Fig. 4 | In-plane magnetization. a Field dependent magnetization curves of $Cr_{1.25}Te_2$ measured at different sample temperatures and the magnetic field applied along the plane of the sample. The non-saturating slopes of the magnetization versus magnetic field curves is a typical sign of antiferromagnetic character. Below the magnetic ordering temperature, several intermediate steps of the spin reorientation process are described in (**b**) Sketch of the spin reorientation mechanism.

surrounding the material's magnetic behavior. We observed abrupt spin-flop transitions, in stark contrast to previous reports of gradual reorientation, and place $Cr_{1+\delta}Te_2$ as a compelling candidate for spin-flop generation and a potential seat for complex spin textures when proximitised with other 2D materials. The robust nature of orthogonal ferromagnetism across varying doping levels underscores its significance in the exploration of emergent quantum phases in low-dimensional materials and enriches our knowledge on unconventional magnetic phases[36–39].

Methods

Growth

To obtain high-quality single crystals, the starting elements were put into a quartz ampule with a capillary bottom. The ampule was evacuated and sealed under a pressure of 2×10^{-7}Torr and placed in a furnace. The furnace was raised to 600 °C and held for 72 h. The furnace temperature was then raised to 1150 °C at a rate of 10 °C/h and soaked for 48 h. For promote the single crystalline growth, the temperature was slowly cooled to room temperature over 10 days.

Photoelectron Spectroscopy

Photoelectron spectroscopy experiments were performed at the CX2 endstation of CASSIOPÉE beamline, SOLEIL synchrotron. The samples were cleaved in ultrahigh vacuum (pressure 1×10^{-10} mbar) and at the temperature of 20 K, which was kept constant throughout the data acquisition. Linearly polarized light (both horizontal and vertical) was varied between 20–90 eV photon energies. Angularly-resolved photoemission spectra were collected by a Scienta R4000 analyzer. The energy and momentum resolutions were better than 15 meV and 0.08 $Å^{-1}$, respectively. The 6-axis manipulator allowed for fine alignment of the sample's high symmetry directions along the analyzer's slit. Spin-ARPES measurements were obtained at Bloch beamline, MAX IV synchrotron.

SQUID measurements

SQUID measurements were performed using a Quantum Design magnetic property measurement system MPMS®3 following standard procedures. Magnetic field sweeps were made in no-overshoot, persistent mode. The curves shown here have been corrected from their diamagnetic signal at high fields. To be the most accurate, we remove the sample holder signal, mainly diamagnetic, by measuring the sample holder without the magnetic sample. We then removed this contribution from the measurement of the crystal.

DFT calculations

The DFT calculations were carried out with the electronic structure package GPAW[40,41] using plane waves and the projector-augmented wave method. For all calculations we used a plane wave cutoff of 800 eV, a uniform k-point grid of $11 \times 11 \times 13$ and a Fermi-Dirac smearing of 10 meV. The structure ($2 \times 2 \times 1$ repetition of the $CrTe_2$ unit cell with a single intercalated atom) was relaxed until all forces were below 0.005 eV/Å using the PBE functional in a collinear magnetic configuration with intercalated atoms being antialigned with ferromagnetic $CrTe_2$ planes. All subsequent calculations were carried out using the LDA functional and non-collinear DFT, including self-consistent spin-orbit. We tested a wide range of different initial non-collinear configurations and found the one shown in Fig. 3 to be the most stable. All calculated band structures were obtained using the PBE functional and unfolded to the primitive unit cell of $CrTe_2$[42]. Spin-orbit coupling was included non-self-consistently in these calculations[43].

Raman spectroscopy

For Raman spectroscopy measurement the wavelength used was 632.81 nm with 10% of the laser power. The objective used was x100 with a grating of 600 mm^{-1}.

Data availability

The data that support the findings of this study are available have at https://doi.org/10.5281/zenodo.15277182[44].

References

1. Chaluvadi, S. K. et al. Uncovering the lowest thickness limit for room-temperature ferromagnetism of $Cr_{1.6}Te_2$. *Nano Lett.* **24**, 7601 (2024).
2. Fujisawa, Y. et al. Widely tunable berry curvature in the magnetic semimetal $Cr_{1+\delta}Te_2$. *Adv. Mater.* **35**, 2207121 (2023).
3. Fujisawa, Y. et al. Tailoring magnetism in self-intercalated in self-intercalated $Cr_{1+\delta}Te_2$ epitaxial films. *Phys. Rev. Mater.* **4**, 114001 (2020).
4. Guillet, Q. et al. Epitaxial van der Waals heterostructures of Cr_2Te_3 on two-dimensional materials. *Phys. Rev. Mater.* **7**, 054005 (2023).

5. Guillet, Q. et al. Magnetic evolution of Cr_2Te_3 epitaxially grown on graphene with post-growth annealing. *Appl. Phys. Lett.* **124**, 202402 (2024).
6. Freitas, D. C. et al. Ferromagnetism in layered metastable 1T-$CrTe_2$. *J. Phys.: Condens. Matter* **27**, 176002 (2015).
7. Purbawati, A. et al. In-plane magnetic domains and Néel-like domain walls in thin flakes of the room temperature $CrTe_2$ van der Waals ferromagnet. *ACS Appl. Mater. Interfaces* **12**, 30702 (2020).
8. Zhang, X. et al. Room-temperature intrinsic ferromagnetism in epitaxial $CrTe_2$ ultrathin films. *Nat. Commun.* **12**, 2492 (2021).
9. Dijkstra, J., Weitering, H. H., van Bruggen, C. F., Haas, C. & de Groot, R. A. Band-structure calculations, and magnetic and transport properties of ferromagnetic chromium tellurides (CrTe, Cr_3Te_4, Cr_2Te_3). *J. Phys.: Condens. Matter* **1**, 9141 (1989).
10. Li, H. et al. Molecular beam epitaxy grown Cr_2Te_3 thin films with tunable Curie temperatures for spintronic devices. *ACS Appl. Nano Mater.* **2**, 6809 (2019).
11. Zhou, J. et al. Structure dependent and strain tunable magnetic ordering in ultrathin chromium telluride. *J. Alloy. Compd.* **893**, 162223 (2022).
12. Li, Q.-Q. et al. Magnetic properties manipulation of $CrTe_2$ bilayer through strain and self-intercalation. *Appl. Phys. Lett.* **119**, 162402 (2021).
13. Lasek, K. et al. Van der Waals epitaxy growth of 2D ferromagnetic $Cr_{(1+\delta)}Te_2$ nanolayers with concentration-tunable magnetic anisotropy. *Appl. Phys. Rev.* **9**, 011409 (2022).
14. Pramanik, T. et al. Angular dependence of magnetization reversal in epitaxial chromium telluride thin films with perpendicular magnetic anisotropy. *J. Magn. Magn. Mater.* **437**, 72 (2017).
15. Coughlin, A. L. et al. Van der Waals superstructure and twisting in self-intercalated magnet with near room-temperature perpendicular ferromagnetism. *Nano Lett.* **21**, 9517 (2021).
16. Chen, J. et al. Evidence for magnetic skyrmions at the interface of ferromagnet/topological-insulator heterostructures. *Nano Lett.* **19**, 6144 (2019).
17. Kushwaha, N. et al. From ferromagnetic semiconductor to antiferromagnetic metal in epitaxial Cr_xTe_y monolayers. Preprint at https://arxiv.org/abs/2409.00189 (2024).
18. Tang, B. et al. Phase engineering of cr5te8 with colossal anomalous Hall effect. *Nat. Electron.* **5**, 224 (2022).
19. Liu, Y., Abeykoon, M., Stavitski, E., Attenkofer, K. & Petrovic, C. Magnetic anisotropy and entropy change in trigonal Cr_5Te_8. *Phys. Rev. B* **100**, 245114 (2019).
20. Varvaro, G. et al. Magnetization reversal mechanism in perpendicular exchange-coupled Fe/$L1_0$FePt bilayers. *N. J. Phys.* **14**, 073008 (2012).
21. Thórarinsdóttir, K. A., Hase, T., Hjörvarsson, B. & Magnus, F. Amorphous exchange-spring magnets with crossed perpendicular and in-plane anisotropies. *Phys. Rev. B* **103**, 014440 (2021).
22. de Sousa, N. et al. Spin configurations in hard/soft coupled bilayer systems: transitions from rigid magnet to exchange-spring. *Phys. Rev. B* **82**, 104433 (2010).
23. Qin, Q., Song, W., He, S., Yang, P. & Chen, J. Magnetization reversal and magnetoresistance behavior of exchange coupled $SrRuO_3$ bilayer. *J. Phys. D: Appl. Phys.* **50**, 215002 (2017).
24. Qin, Q. et al. Interfacial antiferromagnetic coupling between $SrRuo_3$ and $La_{0.7}Sr_{0.3}Mno_3$ with orthogonal easy axis. *Phys. Rev. Mater.* **2**, 104405 (2018).
25. Purbawati, A. et al. Stability of the in-plane room temperature van der Waals ferromagnet chromium ditelluride and its conversion to chromium-interleaved $CrTe_2$ compounds. *ACS Appl. Electron. Mater.* **5**, 764 (2023).
26. Di Sante, D. et al. Flat band separation and robust spin Berry curvature in bilayer kagome metals. *Nat. Phys.* **19**, 1135 (2023).
27. Bigi, C. et al. Electronic structure of intertwined kagome, honeycomb, and triangular sublattices of the intermetallics mco_2al_9 (m = sr, ba). *Phys. Rev. B* **108**, 075148 (2023).
28. Mazzola, F. et al. Observation of termination-dependent topological connectivity in a magnetic Weyl Kagome lattice. *Nano Lett.* **23**, 8035 (2023).
29. Mazzola, F. et al. Unveiling the electronic structure of pseudotetragonal WO_3 thin films. *J. Phys. Chem. Lett.* **14**, 7208 (2023).
30. Mazzola, F. et al. Discovery of a magnetic Dirac system with a large intrinsic nonlinear Hall effect. *Nano Lett.* **23**, 902 (2023).
31. Mazzola, F. et al. Disentangling structural and electronic properties in V_2O_3 thin films: a genuine nonsymmetry breaking Mott transition. *Nano Lett.* **22**, 5990 (2022).
32. Fabre, F. et al. Characterization of room-temperature in-plane magnetization in thin flakes of $CrTe_2$ with a single-spin magnetometer. *Phys. Rev. Mater.* **5**, 034008 (2021).
33. Durhuus, F. L., Skovhus, T. & Olsen, T. Plane wave implementation of the magnetic force theorem for magnetic exchange constants: application to bulk Fe, Co and Ni. *J. Phys.: Condens. Matter* **35**, 105802 (2023).
34. Tan, C. et al. Hard magnetic properties in nanoflake van der Waals Fe_3GeTe_2. *Nat. Commun.* **9**, 1554 (2018).
35. Ikeda, S. et al. A perpendicular-anisotropy CoFeB–MgO magnetic tunnel junction. *Nat. Mater.* **9**, 721 (2010).
36. Mazzola, F. et al. Signatures of a surface spin–orbital chiral metal. *Nature* **626**, 752–758 (2024).
37. Mazzola, F. et al. Anomalous spin-optical helical effect in Ti-based kagome metal. Preprint at https://arxiv.org/abs/2502.19589 (2025).
38. Vita, A. D. et al. Optical switching in a layered altermagnet. Preprint at https://arxiv.org/abs/2502.20010 (2025).
39. Candelora, C. et al. Discovery of intertwined spin and charge density waves in a layered altermagnet. Preprint at https://arxiv.org/abs/2503.03716 (2025).
40. Enkovaara, J. et al. Electronic structure calculations with GPAW: a real-space implementation of the projector augmented-wave method. *J. Phys.: Condens. Matter* **22**, 253202 (2010).
41. Mortensen, J. J. et al. GPAW: an open Python package for electronic structure calculations. *J. Chem. Phys.* **160**, 092503 (2024).
42. Popescu, V. & Zunger, A. Extracting E versus K - effective band structure from supercell calculations on alloys and impurities. *Phys. Rev. B - Condens. Matter Mater. Phys.* **85**, 1 (2012).
43. Olsen, T. Designing in-plane heterostructures of quantum spin Hall insulators from first principles: $1T' - MoS_2$ with adsorbates. *Phys. Rev. B* **94**, 235106 (2016).
44. Bigi, C. et al. Data: Bilayer orthogonal ferromagnetism in CrTe2-based van der Waals system, *Zenodo*, https://doi.org/10.5281/zenodo.15277182 (2025).
45. Fu, B., Bao, X., Deng, H. & Zhang, M. Redetermination the basic cell trigonal Cr_5Te_8 single crystal structure and its temperature dependence Raman spectra. *J. Solid State Chem.* **300**, 122222 (2021).

Acknowledgements

The authors acknowledge M. Brissaud for assistance during some photoelectron spectroscopy measurements. We acknowledge SOLEIL for provision of synchrotron radiation facilities under proposal number 20240527. F.M. greatly acknowledges the SoE action of PNRR, number SOE_0000068 and the funding by the European Union - NextGenerationEU, M4C2, within the PNRR project NFFA-DI, CUP B53C22004310006, IR0000015. This work was supported by the National Research Foundation of Korea (NRF) funded by the Ministry of Education, Science and Technology (NRF-2019M2C8A1057099 and NRF-2022R1I1A1A01063507). J.A.M. acknowledges support from DanScatt (7129-00011B). M. L. and T.B. acknowledge the MAX IV Laboratory for beamtime on the Bloch beamline. Research conducted at MAX IV,

a Swedish national user facility, is supported by Vetenskapsrådet (Swedish Research Council, VR) under contract 2018-07152, Vinnova (Swedish Governmental Agency for Innovation Systems) under contract 2018-04969 and Formas under contract 2019-02496. H.T. and T.J. acknowledge the support of the French National Research Agency (ANR) (MOSAICS project, ANR-22-CE30-0008). This work was also supported by ANR through the France 2030 PEPR SPIN government grant ANR-22-EXSP 0007. C.J., V.P. and M.J. were supported by the FLAG-ERA grant MNEMOSYN. They also acknowledge the French National Research Agency (ANR) for its support through the ANR-18-CE24-0007 MAGIC-VALLEY, ANR-20-CE24-0015 ELMAX and ESR/EQUIPEX+ ANR-21-ESRE-0025 2DMAG projects. ADV acknowledges funding from the Deutsche Forschungsgemeinschaft (DFG) within Transregio TRR 227 Ultrafast Spin Dynamics, the Max Planck Society and the Berlin Quantum Initiative.

Author contributions

F.M. conceived the project. Y.H. grew the samples and performed the structural characterization. C.B., F.M., A.D.V., T.J., H.C.T., F.B., P.L.F., P.T., J.A.M., O.J.C., S.K.C., P.O., and M.C. performed the ARPES experiments, and C.B. and F.M. analyzed the data. M.L., T.B., A.J., and F.M. performed the spin-ARPES investigation. M.J., C.J., V.P., and J.F.J. performed the magnetic measurements and analyzed the data. T.O. performed the DFT calculations, C.B., V.P., T.O., M.J., and F.M. wrote the manuscript with inputs from all the coauthors.

Competing interests

The authors declare no competing interests.

Additional information

Supplementary information The online version contains supplementary material available at https://doi.org/10.1038/s41467-025-59266-4.

Correspondence and requests for materials should be addressed to Chiara Bigi, Thomas Olsen, Younghun Hwang, Matthieu Jamet or Federico Mazzola.

Peer review information *Nature Communications* thanks Yi Zhang and the other, anonymous, reviewer(s) for their contribution to the peer review of this work. A peer review file is available.

[1]Synchrotron SOLEIL, Saint-Aubin, France. [2]Univ. Grenoble Alpes, CEA, CNRS, IRIG-SPINTEC, Grenoble, France. [3]Université Paris-Saclay, UVSQ, CNRS, GEMaC, Versailles, France. [4]Fritz Haber Institut der Max Planck Gesellshaft, Faradayweg 4–6, Berlin, Germany. [5]Ultrafast Nanoscience Group, Institute for Physics and Astronomy, Technical University Berlin, Straße des 17. Juni 135, Berlin, Germany. [6]Univ Rennes, IPR Institut de Physique de Rennes, UMR 6251, Rennes, France. [7]Univ. Grenoble Alpes, CEA, CNRS, IRIG-SYMMES, Grenoble, France. [8]Department of Physics and Astronomy, Interdisciplinary Nanoscience Center, Aarhus University, Aarhus C, Denmark. [9]School of Physics and Astronomy, Monash University, Clayton, Vic, Australia. [10]CNR-IOM Istituto Officina dei Materiali, Trieste, Italy. [11]CNR-SPIN, c/o Universitá di Salerno, Fisciano (SA), Italy. [12]MAX IV Laboratory, Lund University, Lund, Sweden. [13]CAMD, Computational Atomic-Scale Materials Design, Department of Physics, Technical University of Denmark, Kongens Lyngby, Denmark. [14]Electricity and Electronics and Semiconductor Applications, Ulsan College, Ulsan, Republic of Korea. [15]Department of Molecular Sciences and Nanosystems, Ca Foscari University of Venice, Venice, Italy. [16]CNR-SPIN UOS Napoli, Complesso Universitario di Monte Sant'Angelo, Via Cinthia, Napoli, Italy. [17]These authors contributed equally: Chiara Bigi, Cyriack Jego, Vincent Polewczyk. ✉e-mail: chiara.bigi@synchrotron-soleil.fr; tolsen@fysik.dtu.dk; younghh@uc.ac.kr; matthieu.jamet@cea.frt; federico.mazzola@spin.cnr.it